Journal of Thermal Analysis and Calorimetry, Vol. 87 (2007) 1, 277–284

DSC ANALYSIS OF STRENGTHENING PRECIPITATES IN ULTRAFINE Al–Mg–Si ALLOYS

M. Vedani[1], *G. Angella*[2], *Paola Bassani*[3*], *D. Ripamonti*[1] *and A. Tuissi*[3]

[1]Politecnico di Milano, Dipartimento di Meccanica, Via La Masa 34, 20156 Milano, Italy
[2]National Research Council, Institute for Energetics and Interphases CNR-IENI, Via R. Cozzi 53, 20125 Milano, Italy
[3]National Research Council, Institute for Energetics and Interphases CNR-IENI, Corso Promessi Sposi 29, 23900 Lecco, Italy

Equal channel angular pressing (ECAP) was carried out on solution annealed samples of Al–Mg–Si–Zr and Al–Mg–Si–Zr–Sc alloys to achieve a substantial grain refinement of the materials. Post ECAP aging was then investigated on the ultrafine grained alloys by DSC and TEM analyses.

DSC scans were carried out with heating rates ranging from 5 to 30°C min^{-1}. Peak identification was performed by the support of literature information and TEM analyses. Precipitation kinetics revealed to be similar for both alloys but the Sc-free alloy showed a recrystallization peak at temperatures ranging from 310 to 340°C, depending on the strain accumulated during ECAP. On the contrary, the Sc-containing alloy showed a greater grain stability. Analyses of peak positions and of activation energies as a function of ECAP passes experienced by the samples revealed large modifications of precipitation kinetics in the ultrafine-grained alloys with respect to the coarse-grained materials.

Keywords: *aging behaviour, Al–Mg–Si alloys, ECAP, scandium, ultra-fine grained alloys*

Introduction

Al–Mg–Si alloys are an important group of materials, widely used for demanding structural applications. Their age hardening response can be very significant, leading to remarkable improvement of strength after an appropriate heat treatment. The precipitation sequence of Al–Mg–Si alloys has been studied for many years but only in recent times a satisfactory agreement on phase evolution occurring during aging has been achieved [1–7]. A large number of wrought Al–Mg–Si alloys contain an excess of Si, above that required to form Mg_2Si, to improve the age hardening response. For these alloys the accepted precipitation sequence starting from a supersaturated solid solution is: separate clusters of Si and of Mg atoms; co-clusters containing Mg and Si atoms; spherical GP zones; needle like metastable β" phase; rod like metastable β' phase; Si precipitates; platelets of equilibrium β phase (Mg_2Si). Among these, the β" precipitates are considered to give the main contribution to strength and hence they are mostly responsible for the maximum age hardening effect [2, 4, 5].

It was also reported that the β" precipitates form by direct nucleation from the GP zones. The distribution and density of the main strengthening particles is therefore largely affected by the structure formed during a pre-aging stage then can occur even at room temperature [6]. High-resolution electron microscopy analyses also revealed that, in addition to the metastable β' phase, other types of precipitates can exist at an advanced stage of aging. The type-B precipitate is reported to appear at the same time of β' during aging. In a subsequent stage, these phases tend to be replaced by the type-A precipitates and by a small fraction of the so-called type-C precipitates, before reaching the overaged condition where Mg_2Si and Si are the predominant phases [3].

Several research works also suggest that the precipitation sequence and kinetics are deeply changed when the alloy structure is plastically deformed. Zhen *et al*. [5, 8] showed that when Al–Mg–Si alloys had been extensively cold rolled and solution treated for short periods, their curves collected during aging featured a decrease of the precipitation temperatures of some phases. It was suggested that the increased density of defects in the crystal structure would enhance appreciably the diffusion distance of Si and hence promote the formation of a more obvious peak for the GP zones, the anticipation of the metastable β"/β' peak temperatures and the reduction of the amount of Si and Mg_2Si phases that eventually formed.

Similar modifications in the precipitation sequence were also found in alloys deformed in the severe plastic deformation (SPD) regime at moderate temperatures, to produce ultrafine grained alloys by a continuous

* Author for correspondence: bassani@ieni.cnr.it

1388–6150/$20.00

Akadémiai Kiadó, Budapest, Hungary
Springer, Dordrecht, The Netherlands

recrystallization process [9, 10]. The issue of precipitate evolution in SPD processed microstructures is of great importance because, even though remarkable properties can be achieved directly after SPD, it is only by an appropriate aging treatment after the grain refining process that ultra-high strength levels exceeding 600 MPa can be achieved in Al alloys.

Murayama *et al*. [11] investigated a solution treated Al–Cu binary alloy processed by equal channel angular pressing (ECAP) to refine its structure at room temperature. By careful DSC and TEM analyses they stated that during post-ECAP aging, the formation of GP zones and of transition θ" precipitates was suppressed and that the precipitation of θ' and θ phases was enhanced and occurred at lower temperatures in the heavily deformed structure of the alloys. Investigations on other aluminium alloys also confirmed accelerated kinetics of the aging processes [12–14].

The use of stable dispersoid forming elements in aluminium alloys to be processed by SPD has attracted the attention of researchers in view of the possibility of increasing the resistance to recrystallization of the ultrafine grained alloys during high temperature service or post-SPD heat treatments. Scandium represents one of the most powerful elements from this perspective since the resulting precipitation of coherent Al_3Sc ($L1_2$ type crystals) particles is able to retain the original deformed microstructure of the alloy even after high-temperature annealing [15–18]. It is also well accepted that the effect of Sc is amplified by the simultaneous presence of Zr, giving rise to the formation of complex $Al_3(Sc_xZr_{1-x})$ precipitates.

From recent research works, it was also confirmed that Sc/Zr-modified Al alloys can be effectively refined to submicrometer grain-size levels by severe plastic deformation (SPD) techniques and that the produced microstructure retains a reasonably high thermal stability [19–26].

In the present study a combined investigation is presented on aging behaviour of experimental Al–Mg–Si alloys processed by ECAP at different levels of strain, pertaining to the SPD regime. The effect of the different amount of stabilizing dispersoids is considered by investigating two materials modified by Zr and Zr+Sc addition.

Experimental

Materials

Two experimental Al–Mg–Si–Zr alloys supplied in the form of extruded bars with a diameter of 10 mm were investigated. Their chemical composition is given in Table 1. The first alloy is to be considered as a standard 6082 alloy modified by the addition of 0.10% Zr while the second material represents a modified version of the former, obtained by a further addition of 0.12% Sc.

Samples of the alloys were cut into cylinders having a length of 100 mm, solution treated in a muffle furnace at 530°C for 1.5 h, water quenched and stored at about –5°C to prevent significant artificial aging to occur before testing.

ECAP was carried out at room temperature, using a die with channels intersecting at an angle Φ=90° and with an external curvature angle Ψ=20°, corresponding to a theoretical strain of 1.05 at each pass [27]. Samples were processed by the so-called route C (rotation by 180° of the specimen at each pass) to accumulate up to six passes, for a total equivalent strain of 6.3.

Analyses on grain structure evolution after SPD and on precipitates developed during aging was carried out on ECAP processed and post-ECAP aged samples of the two alloys by transmission electron microscopy (TEM). Samples were prepared by longitudinally cutting 1 mm thick disks from the billets, manually grinding and polishing. Twin jet electrolytic thinning was then carried out at –35°C with a 30% HNO_3 solution in methanol at 18 V.

Samples of the processed alloys were also subjected to differential scanning calorimetry (DSC) analyses to investigate the influence of SPD on phase precipitation during aging. Specimens were cut from bulk samples with a metallographic diamond cutting saw, and grounded with emery papers to final flat cylinder shape. The final mass of each DSC sample was about 100 mg.

Tests have been performed with a Setaram Labsys TG-DTA system, equipped with a detector configured for DSC analysis in a temperature range from *rT* up to 800°C, using alumina crucibles. Temperature and heat flow calibration has been carried out using pure indium and zinc melting points. The heating chamber was fluxed with argon. The sample mass was checked before and after DSC runs with a

Table 1 Chemical composition (mass%) of the alloys investigated

Material	Mg	Si	Fe	Mn	Zr	Sc	Al	Excess Si
Al–Mg–Si	0.34	0.51	0.16	0.014	0.10	–	bal.	0.27
Al–Mg–Si–Sc	0.36	0.50	0.14	0.013	0.10	0.12	bal.	0.26

high accuracy balance. No significant increase of the mass was observed. Tests were performed by heating at 5–10–20–30°C min^{-1}, and then by cooling to *rT* at 30°C min^{-1} in all cases. Scans test were replicated for the as solubilized material, revealing good repeatibility of the curves. The effects associated to transformation reactions were isolated by subtracting, with instrument software, a baseline of a high purity aluminium run. In addition, TEM observations were carried out on thin discs cut from the ECAP processed billets that underwent interrupted temperature ramps in the DSC apparatus, up to the level corresponding to appearance of the main precipitation peaks. This method allowed achieving a direct comprehension of the possible modification of aging sequence as induced by SPD processing and by the presence of Sc/Zr dispersoids.

The set of DSC data obtained at different heating rates for each material condition were further analysed using a isoconversional analysis. Isoconversional methods allow evaluating the Arrhenius parameters of a reaction independently from the reaction model [28–31]. In particular, according to the Kissinger method, the set of DSC data collected at different heating rates for each material condition can be analysed starting from the fundamental kinetic Eq. (1),

$$d\alpha/dt = k(T)f(\alpha) \quad (1)$$

where t, α, $k(T)$, $f(\alpha)$ are time, extent of conversion, rate constant, reaction model, respectively. $k(T)$ is generally expressed by the Arrhenius equation:

$$k(T) = A\exp(-E_a/RT) \quad (2)$$

where A, E_a, R are Arrhenius pre-exponential factor, activation energy, gas constant in the order.

In the case of constant heating rate tests, the following relation can be derived:

$$\ln(T_p^2/\phi) + E_a/RT_P = \text{constant} \quad (3)$$

where ϕ, T_P are heating rate and peak temperature of a defined transformation, respectively.

Once the experimental data are plotted in the form $\ln(T_p^2/\phi)$ *vs*. $1/T$ given by Eq. (3), E_a can be readily evaluated.

Results

The typical structure of the two alloys after the solution treatment and before ECAP processing is depicted in the optical micrographs given in Fig. 1. The Al–Mg–Si–Zr alloy featured a fully recystallized coarse grain structure whereas the Al–Mg–Si–Zr–Sc alloy maintained the elongated grain structure inherited from the extrusion. TEM observations also showed that a substructure made up of well recovered subgrains free from dislocations at their interiors was present in both the solution treated alloys.

Details about the evolution of the grain structure with increasing ECAP passes have already been given elsewhere [24]. Both alloys underwent similar structural changes by increasing severe plastic deformation, and developed a significantly refined grain structure according to the well established mechanisms [32–34]. Figure 2 demonstrates that already after four passes, an ultrafine grain structure was formed in both alloys.

DSC scans were recorded for the different materials and SPD conditions at four different heating rates, from 5 to 30°C min^{-1}. Figure 3 reports a collection of the heating curves for the as solution treated (0 ECAP passes) Al–Mg–Si–Zr alloy. Curves were shifted along *y*-axis to help data observation. The best resolution and heat flow signal was achieved at the rates of 10 and 20°C min^{-1}. Interpretation of the aging peaks and comparisons among different materials will therefore be carried out mainly by referring to these data.

Figures 4 and 5 summarize the modification of the DSC results as a function of ECAP passes for the two materials investigated. Interpretation of the precipitation and dissolution peaks can be made on the basis of strong similarities found in the DSC curves of Al–Mg–Si alloys with excess of Si published in literature [1, 2, 4, 5, 7, 8]. Considering the curves for 0 ECAP passes, the broad exothermic peaks at about 270°C (upward peaks in the figures) has to be interpreted as two partially superimposed sub-peaks that correspond to the formation of the β" and β' metastable phases at temperatures of 250 and 280°C, respectively. A broad dissolution endothermic peak (downward peak in the figures) of the above phases

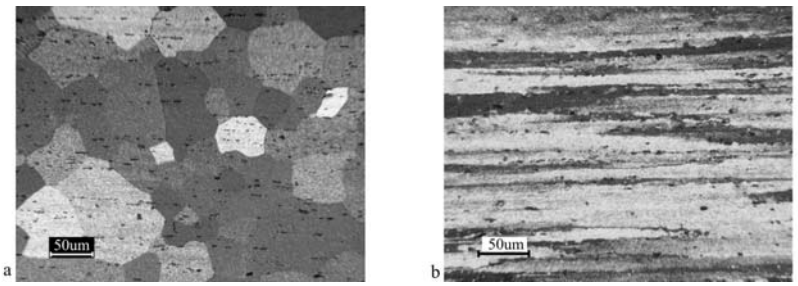

Fig. 1 Representative optical micrographs of longitudinal sections of a) Al–Mg–Si–Zr and b) Al–Mg–Si–Zr–Sc alloys

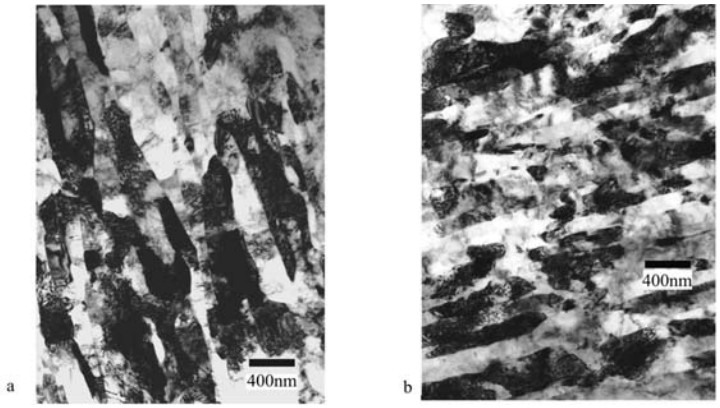

Fig. 2 TEM micrographs of a) Al–Mg–Si–Zr and b) Al–Mg–Si–Zr–Sc alloys after 4 ECAP passes

appear at about 380°C while the second marked exothermic peak at 420°C and the corresponding dissolution peak at 470–480°C are related to formation and dissolution of the equilibrium β-Mg_2Si phase.

The ECAP processed alloys feature marked differences in the position and shape of the peaks. The above mentioned partially superimposed peaks accounting for the formation of β" and β' precipitates now appear as a more narrow peak occurring at 240°C, irrespective of number of ECAP passes and alloy composition. The formation of the stable β precipitates in the severely deformed alloys reveals to be markedly anticipated and of decreasing intensity with increasing number of ECAP passes (compare to the reference peak at 420°C of the undeformed alloys). Finally, it is worth noting that a new peak appears in the temperature range 310–340°C for the ECAP processed Al–Mg–Si–Zr alloy (Fig. 4). The heat flow released apparently increases with increasing number of passes whereas the peak temperature moves from 340°C of the sample processed to a single pass, down to 310°C for the sample processed to four passes.

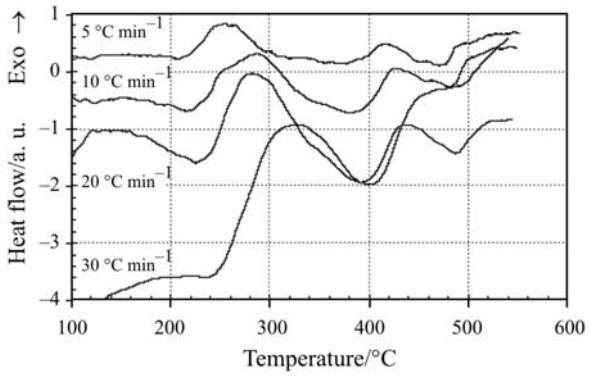

Fig. 3 DSC curves of the solution treated Al–Mg–Si–Zr alloy. Curves are shifted along *y*-axis to reduce superimposition

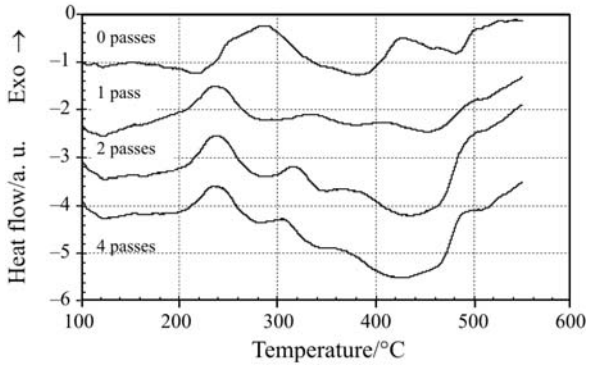

Fig. 4 DSC curves of the Al–Mg–Si–Zr alloy as a function of ECAP passes (heating rate 10°C min^{-1}). Curves are shifted along *y*-axis to avoid superimposition

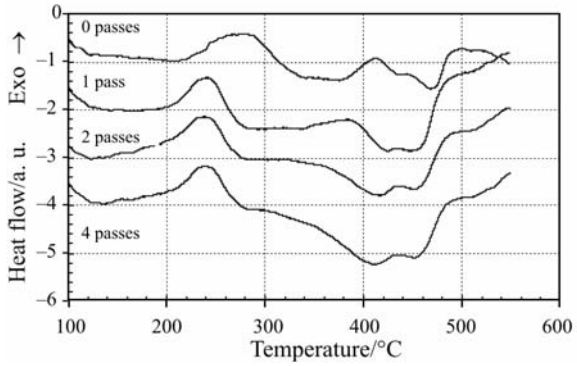

Fig. 5 DSC curves of the Al–Mg–Si–Zr–Sc alloy as a function of ECAP passes (heating rate 10°C min^{-1}). Curves are shifted along *y*-axis to avoid superimposition

Figure 6 depicts the precipitate structure observed by TEM for the two solution treated alloys (0 ECAP passes) aged up to 350°C in the DSC. Their structural condition reproduces that found just at the end of the broad peak in both alloys and roughly corresponds to the peak-aged condition produced in industrially treated alloys. β"/β' needle-shaped precipitates aligned along the $<100>_{Al}$ direction can be identified in the aged matrix structures. In addition, in the Sc-containing alloy (Fig. 6b) a large number of coherent $Al_3(Sc_xZr_{1-x})$ type dispersoids are observed. The introduction of ECAP processing after the solution treatment but before aging up to the first peak of the β"/β' phases led to the structure shown in Fig. 7. Inspection of the TEM micrographs reveals that aging

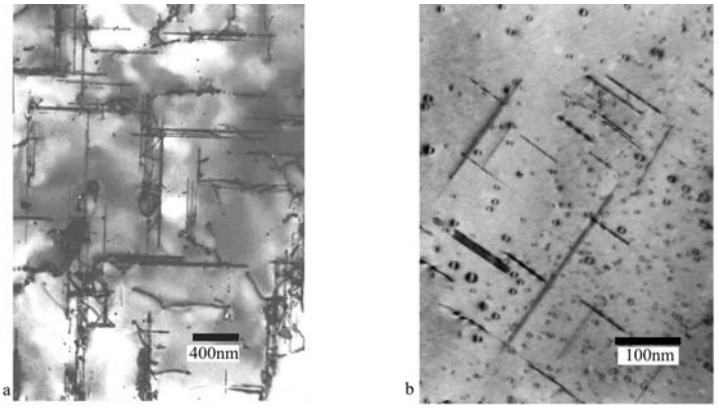

Fig. 6 Precipitate structure of the alloys after solution treatment and aging up to 350°C; a) Al–Mg–Si–Zr, b) Al–Mg–Si–Zr–Sc

in the DSC up to the temperature of 300°C did not modify significantly the ultrafine grain structure achieved by SPD (Fig. 7a). In both alloys, the strengthening precipitates maintained their needle-like shape and the $<100>_{Al}$ direction but the average size (here evaluated only qualitatively) and volume fraction were remarkably reduced (Fig. 7b).

The analysis of the DSC curves revealed an unexpected peak in the range 340–310°C of the ECAP processed Al–Mg–Si–Zr samples. Figure 8 depicts TEM images taken on samples aged in the DSC immediately before the onset and after the offset of this peak. The changes observed in the grain structure of the Sc-free alloy clearly demonstrated that the alloy underwent a recrystallization process in this temperature range.

In Table 2 the data about peak temperatures and activation energies evaluated by the Kissinger method are summarized for the transformations of greater interest for this study. Data about the coefficient of regression R that was used to calculate the activation energy are also given as a further parameter for data evaluation. For both alloys it is shown that the β”/β’ precipitation peak temperatures clearly decrease when ECAP is carried out before aging, but no significant effect due to the amount of plastic deformation given by ECAP can be noticed from the figures (compare the T_p data for 1, 2 and 4 passes). The calculated values of activation energies of the solution treated alloys (0 ECAP passes) have to be regarded with caution since during the analysis it was not possible to resolve the broad β”/β’ peak into the two distinct peaks. In addition, in several curves, uncertainties have been found in the identification of the baseline and therefore in the definition of onset and offset temperatures of the peaks. The low value of the coefficient of regression R also confirms the uncertainties that have been encountered when trying to analyse the two superimposed peaks.

Table 2 further confirms that the formation of the stable β-Mg_2Si phase occurs at increasingly lower temperatures when increasing the number of ECAP passes. Correspondingly, the activation energy values tend to decrease. It is also worth considering that in the Sc-containing alloy, the β transformation systematically occurs at lower temperatures and by reduced activation energies with respect to the Sc-free alloy.

Finally, the recrystallization peak that was noticed only in the Al–Mg–Si–Zr alloy features decreasing peak temperatures with ECAP passes and a con-

Table 2 Peak temperatures and activation energies evaluated form DSC runs

	Passes	Al–Mg–Si–Zr				Al–Mg–Si–Zr–Sc			
		0	1	2	4	0	1	2	4
β’’/β’	T_p (10°C min^{-1})/°C	288.3	235.8	237.6	239.7	283.2	243.1	237.4	239.8
	T_p (20°C min^{-1})/°C	283.7	257.6	255.4	254.5	275.6	257.6	255.3	255.0
	E_a/kJ mol^{-1}	71.9	84.7	96.7	95.7	101.7	78.9	85.8	86.2
	R	0.84	0.98	0.97	0.98	0.85	0.99	0.99	0.99
β	T_p (10°C min^{-1})/°C	424.1	414.5	385.8	369.4	413.2	385.9	357.9	349.1
	T_p (20°C min^{-1})/°C	432.8	424.5	403.8	385.0	422.4	402.8	388.1	359.8
	E_a/kJ mol^{-1}	223.8	166.7	138.0	162.5	215.8	150.7	103.8	75.3
	R	0.98	0.99	0.99	0.94	0.99	0.95	0.96	0.94
RX	T_p (10°C min^{-1})/°C		335.4	319.4	308.5				
	T_p (20°C min^{-1})/°C		359.5	332.8	318.5				
	E_a/kJ mol^{-1}		129.9	124.7	132.7				
	R		0.95	0.99	0.98				

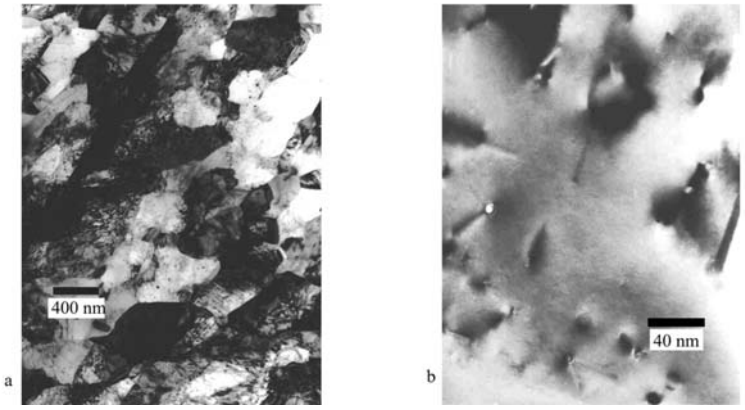

Fig. 7 Structure of the Al–Mg–Si–Zr–Sc alloy after solution treatment, ECAP processing to four passes and aging up to 300°C; a) grain structure, b) precipitate morphology

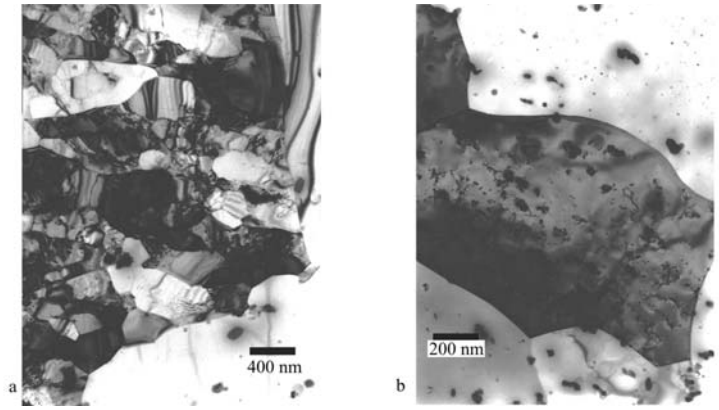

Fig. 8 Structure of the Al–Mg–Si–Zr alloy after solution treatment, ECAP processing to four passes and aging a) up to 280 and b) 350°C

stant activation energy, in good agreement with established physical laws on recrystallization process of workhardened metals.

Discussion

A large number of literature reports is currently available on synthesis and properties of ultrafine and nanocrystalline metallic alloys produced by SPD. Their remarkably high mechanical properties are basically explained by the strengthening due to grain refinement and partly due to dislocation strengthening [9, 10]. Precipitation strengthening is a further mechanisms available to create obstacle for plastic deformation and hence to attain even higher performance in ultrafine and nanostructured alloys. Indeed, recent works showed that a pre-ECAP solution treatment combined with post-ECAP low-temperature aging is very effective in enhancing the room temperature strength of Al–Cu and Al–Mg–Si commercial alloys [12–14, 35, 36]. However, all the available experimental data show that the aging kinetics of SPD processed alloys is significantly accelerated. This phenomenon is generally accounted for by the large fraction of non-equilibrium grain boundaries found in the ultrafine metal structure and in the large fraction of lattice defects that dramatically increase the diffusivity of alloying elements.

The DSC analyses presented in this study confirmed that the aging kinetics and precipitation sequence in Al–Mg–Si–Zr alloys is clearly altered by ECAP processing. A proposed interpretation of the peak modification and shift found in the deformed alloys can be based on speculations about the Mg–Si balance in the alloy compositions. Gupta *et al*. [1] already noted that an increase in the excess of Si with respect to that required to form stoichiometric Mg_2Si, made the two subpeaks related to the formation of β" and β' more resolved and progressively suppressed the formation of the stable β peak during the last stages of aging. In the alloys of the present work, the excess of Si estimated according to [1] is of the order of 0.27%, as opposed to more than 1% excess Si considered in the study of Gupta *et al*. [1]. However, it is believed that the increased atom mobility in the disordered SPD structure, not only accelerates the aging kinetics but would also emphasize compositional effects such as those concerned with the Mg–Si balance. From the combined analysis of DSC curves and TEM micrographs presented in this work, it can be supposed

that, owing to the higher Si amount available due to increased diffusivity, only the β" phase would form during post-ECAP aging of the samples, while the precipitation of β' is suppressed or at least strongly reduced. The reduction of the β' precipitates in alloys with excess Si was also stated by Matsuda *et al*. [3]. These authors demonstrated that in such alloys, Si-rich metastable phases (type-B and type-A) are formed as a competing phase to β', and that the possible depletion in Si from the matrix could also reduce the formation of the stable β-Mg_2Si phase.

A further important aspect to be considered concerns the effects of Sc in the alloy composition. There is a good agreement in literature on the increased grain stability and the acceleration of the refinement mechanism in SPD processed Al alloy containing Sc and Zr+Sc. These statements are confirmed also by the present study since a recrystallization peak was found only in the DSC curve of the Sc-free alloy. It was thus confirmed that the combination of Zr+Sc can effectively control the grain size of the structure during the post-ECAP aging process.

A further question arises on the possible interrelation that could exist between the effects of the coherent $Al_3(Sc_xZr_{1-x})$ type dispersoids controlling recrystallization and grain size and the aging process. For this purpose, a detailed analysis was carried out on the positions and related activation energies of the DSC peaks. Taking into account the formation of β" and β' precipitates that are responsible of the peak hardness of the Al–Mg–Si alloys, it is possible to state that Sc does not have any significant effect. Both peak temperatures and activation energies have comparable values, irrespective of the presence of Sc in the alloy.

On the contrary, Sc appears to be responsible of slight modifications detected in the precipitation of the β-Mg_2Si phase, which would correspond to extensive overaging of the alloys. Although the general trend of peak characteristics as a function of ECAP passes is maintained, it can be stated that the presence of Sc induces a reduction of the β peak temperatures and of the activation energies. Deeper analyses would be required to clarify this point, but it could be supposed that nucleation of the β phase could be favoured by the $Al_3(Sc_xZr_{1-x})$ precipitates. This statement is also supported by the fact that increasing the possibility for heterogeneous nucleation of the β phase would be established when the Sc-containing precipitates lose coherency with the Al matrix. Loss of coherency is reported to occur generally at temperatures in the range 400–450°C [16, 18]. It is also expected that increased lattice strain, as induced by increasing ECAP passes, would progressively anticipate this critical temperature, in accordance to the measured trend.

Conclusions

The aging behaviour of ultrafine Al–Mg–Si–Zr and Al–Mg–Si–Zr–Sc alloys was investigated by DSC and TEM analyses. Different amounts of plastic deformation were given by ECAP to the solution treated alloys. Post-ECAP aging studies were then carried out to investigate the effect of severe plastic deformation on aging kinetics and precipitation sequence. The results allowed to draw the following conclusions.

- Analyses of the peak positions, activation energies and precipitate morphology as a function of ECAP passes experienced by the samples revealed large modifications of precipitation kinetics in the ultrafine-grained alloys with respect to the coarse-grained materials.
- The precipitation of the β" and β' phases occurred at significantly lower temperatures with increasing ECAP strain. It was also supposed that the formation of the β' precipitates is suppressed or at least strongly reduced due to expected precipitation of competing Si-rich phases in the heavily deformed alloy structure.
- Formation of the stable β precipitates during aging of the severely deformed alloys revealed to be markedly anticipated and of decreasing intensity with increasing number of ECAP passes, owing to Si depletion from the matrix.
- The presence of Sc did not affect significantly the precipitation behaviour in the transformation range concerned with peak aging treatments. On the contrary, Sc promoted slight modifications in the precipitation of the β-Mg_2Si phase, which corresponds to extensive overaging of the alloys. The reduction of the β peak temperatures and of the related activation energies were tentatively accounted for by increased nucleation favoured by the $Al_3(Sc_xZr_{1-x})$ precipitates.
- The Sc-free alloy showed a recrystallization peak at temperatures ranging from 310 to 340°C, depending on the strain accumulated by ECAP, while the Sc-containing alloy showed a greater grain stability.

Acknowledgements

The authors would like to thank Dr. E. Festari and Mr. P. Pellin for their skilful contribution to the experimental work.

References

1 K. Gupta, D. J. Lloyd and S. A. Court, Mater. Sci. Eng., A316 (2001) 11.
2 G. A. Edwards, K. Stiller, G. L. Dunlop and M. J. Couper, Acta Mater., 46 (1998) 3893.

3 K. Matsuda, Y. Sakaguchi, Y. Miyata, Y. Uetani, T. Sato, A. Kamio and S. Ikeno, J. Mater. Sci., 35 (2000) 179.
4 M. Ta Eda, F. Oh Ubo and T. Shirai, J. Mater. Sci., 33 (1998) 2385.
5 L. Zhen, W. D. Fei, S. B. Kang and H. W. Kim, J. Mater. Sci., 32 (1997) 1895.
6 M. Murayama and K. Hono, Acta Mater., 47 (1999) 1537.
7 G. Biroli, G. Caglioti, L. Martini and G. Riontino, Scripta Mater., 39 (1998) 197.
8 S. B. Kang, L. Zhen, H. W. Kim and S. T. Lee, Mater. Sci. Forum, 217–222 (1996) 827.
9 R. Z. Valiev, R. K. Islamgaliev and I. V. Alexandrov, Prog. Mater. Sci., 45 (2000) 103.
10 M. A. Meyers, A. Mishra and D. J. Benson, Prog. Mater. Sci., 51 (2006) 427.
11 M. Murayama, Z. Horita and K. Hono, Acta Mater., 49 (2001) 21.
12 J. K. Kim, H. G. Jeong, S. I. Hong, Y. S. Kim and W. J. Kim, Scripta Mater., 45 (2001) 901.
13 W. J. Kim, C. S. Chung, D. S. Ma, S. I. Hong and H. K. Kim, Scripta Mater., 49 (2003) 333.
14 G. Angella, P. Bassani, A. Tuissi and M. Vedani, Mater. Trans., 45 (2004) 2282.
15 V. Ocenasek and M. Slamova, Mater. Charact., 47 (2001) 157.
16 M. J. Jones and F. J. Humphreys, Acta Mater., 51 (2003) 2149.
17 V. G. Davydov, T. D. Rostova, V. V. Zakharov, Y. A. Filatov and V. I. Yelagin, Mater. Sci. Eng., A280 (2000) 30.
18 J. Royset and N. Ryum, Int. Mater. Rev., 50 (2005) 19.
19 A. Vinogradov, A. Washikita, K. Kitagawa and V. I. Kopylov, Mater. Sci. Eng., A349 (2003) 318.
20 K. Furuno, H. Akamatsu, K. Oh-Ishi, M. Furukawa, Z. Horita and T. G. Langdon, Acta Mater., 52 (2004) 2497.
21 S. Lee, A. Utsunomiya, H. Akamatsu, K. Neishi, M. Furukawa, Z. Horita and T. G. Langdon, Acta Mater., 50 (2002) 553.
22 P. J. Apps, M. Berta and P. B. Prangnell, Acta Mater., 53 (2005) 499.
23 M. Cabibbo, E. Evangelista, C. Scalabroni and E. Bonetti, Mater. Sci. Forum, 503–503 (2006) 841.
24 G. Angella, P. Bassani, A. Tuissi, D. Ripamonti and M. Vedani, Mater. Sci. Forum, 503–503 (2006) 493.
25 K.-T. Park, D.-Y. Hwang, Y.-K. Lee, Y.-K. Kim and D. H. Shin. Mater. Sci. Eng., A341 (2003) 273.
26 D. R. Herling and M. T. Smith, Proc. Int. Symp. Ultrafine Grained Materials, Nashville, March 2000. R. S. Mishra, S. L. Semiatin, C. Suryanarayana, N. N. Thadhani, T. C. Lowe, Eds, TMS publisher, (2000), pp. 411–420.
27 Y. Iwahashi, J. Wang, M. Horita, M. Nemoto and T. G. Langdon, Scripta Mater., 35 (1996) 143.
28 H. Tanaka, Thermochim. Acta, 267 (1995) 29.
29 T. Ozawa, Thermochim. Acta, 355 (2000) 35.
30 M. J. Starink, Thermochim. Acta, 404 (2003) 163.
31 S. Vyazovkin, Thermochim. Acta, 355 (2000) 155.
32 Y. Iwahashi, Z. Horita, M. Nemoto and T. G. Langdon, Acta Mater., 45 (1997) 4733.
33 K. Nakashima, Z. Horita, M. Nemoto and T. G. Langdon, Acta Mater., 46 (1998) 1589.
34 A. Gholinia, P. B. Prangnell and M. V. Markushev, Acta Mater., 48 (2000) 1115.
35 E. Cerri and P. Leo, Mater. Sci. Eng., A410–411 (2005) 226.
36 N. Tsuji, T. Iwata, M. Sato, S, Fujimoto and Y. Minamino, Sci. Techn. Adv. Mater., 5 (2004) 173.

DOI: 10.1007/s10973-006-7837-2